ORIGINAL ARTICLE

Accelerating ferroic ageing dynamics upon cooling

Junyan Zhang[1,2,6], Yunwei Mao[1,2,7], Dong Wang[1,2], Ju Li[1,2,3,4] and Yunzhi Wang[1,2,5]

Once a structural glass is formed, its relaxation time will increase exponentially with decreasing temperature. Thus, the glass has little chance of transforming into a crystal upon further cooling to zero Kelvin. However, a spontaneous transition upon cooling from amorphous to long-range ordered ferroic states has been observed experimentally in ferroelastic, ferroelectric and ferromagnetic materials. The origin for this obvious discrepancy is discussed here conceptually. We present a combined theoretical and numerical study of this phenomenon and show that the diffusive and displacive atomic processes that take place in structural glass and amorphous ferroics, respectively, lead to markedly different temperature-dependent relaxation behaviors, one being 'colder is slower' and the other being 'colder is faster'.

INTRODUCTION

The so-called ferroic glasses,[1] including relaxor ferroelectrics,[2,3] ferromagnetic cluster spin glasses[4] and the most recently proposed ferroelastic strain glasses,[5] all have nanoscale heterogeneities in their corresponding ferroic order parameters (that is, the polarization, magnetization and strain, respectively) and characteristic internal ferroic dynamics that slows down with decreasing temperature, at least within a particular temperature range. By ferroic dynamics, we mean the involvement of long-range electrostatic/magnetostatic/elastic interactions and the absence of atomic diffusion. Even though the slowing down of ferroic dynamics with decreasing temperature seems similar to the relaxation dynamics in supercooled liquids and structural glasses, they are intrinsically different because ferroic phase transition is displacive. Indeed, recent experimental studies on ferroic materials find that an inverse type of dynamics widely exists in ferroic systems, that is, accelerating ferroic dynamics with decreasing temperature. For example, the spontaneous transition of relaxor to ferroelectrics was observed decades ago.[6] Moreover, a so-called 'spontaneous' transition from a strain glass to a strain crystal (martensite) upon cooling has been recently reported and discussed in ferroelastic systems such as Ti-Ni-Fe shape memory alloys and Ni-Co-Mn-Ga systems.[7–9] Despite these extensive experimental studies, the explanation for the accelerating ferroic dynamics with decreasing temperature remains unclear.

In this paper, we provide a combined theoretical and numerical study and show that the atomic processes that take place in structural glass and ferroic glass systems exhibit markedly different temperature-dependent relaxation behaviors, one being 'colder is slower' and the other being 'colder is faster'.

MATERIALS AND METHODS

We consider a generic doped ferroelastic system prototype, and theoretically and numerically investigate its relaxation behavior upon cooling within a wide defect concentration range. The theoretical analysis is based on classical non-equilibrium thermodynamics and kinetic theory, and the details of the analysis are presented in the next section. The numerical simulation is based on the phase field method, which is built on the Landau theory of phase transitions and the phase field micro-elasticity theory.[10–12] The details of the simulation are presented in the Supplementary Information. All of the simulations are carried out in two dimensions for the sake of simplicity because the temperature dependence of the ferroelastic transition kinetics (that is, whether colder is faster or colder is slower) will not change whether the simulation is carried out in two dimensions or in three dimensions. Then, the martensitic volume fraction, domain structure and heat capacity are calculated and analyzed throughout the temperature-induced transitions within a wide defect concentration range.

RESULTS AND DISCUSSION

Theoretical analysis

The overall kinetics of a diffusional phase transformation is typically characterized by a C-shaped curve on the time-temperature-transformation (TTT) diagram (for example, the red curve in Figure 1). The slowing down of the ferroic dynamics can also potentially lead to significant metastability, that is, a system ending up in a quite disordered ferroic state (A, defined as an 'amorphous'

[1]Frontier Institute of Science and Technology, Xi'an Jiaotong University, Xi'an, China; [2]State Key Laboratory for Mechanical Behavior of Materials, Xi'an Jiaotong University, Xi'an, China; [3]Department of Nuclear Science and Engineering, Massachusetts Institute of Technology, Cambridge, MA, USA; [4]Department of Materials Science and Engineering, Massachusetts Institute of Technology, Cambridge, MA, USA and [5]Department of Materials Science and Engineering, The Ohio State University, Columbus, OH, USA
[6]Current address: Department of Chemical Engineering, Northeastern University, Boston, MA 02115, USA.
[7]Current address: Department of Mechanical Engineering, Massachusetts Institute of Technology, Cambridge, MA 02139, USA.
Correspondence: Professor J Li, Department of Nuclear Science and Engineering and Department of Materials Science and Engineering, Massachusetts Institute of Technology, 77 Mass Avenue, Building 24-202, MIT, Cambridge, MA 02139, USA.
E-mail: liju@mit.edu
or Professor Y Wang, Department of Materials Science and Engineering, The Ohio State University, 490 Watts Hall, 2041 College Road, Columbus, OH 43210, USA.
E-mail: wang.363@osu.edu

2
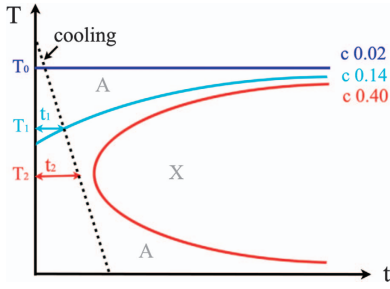
Figure 1 Schematic time-temperature-transformation (TTT) curves for ferroelastic systems with three typical doping levels (mole fraction $c = 0.02$, 0.14 and 0.40). The vertical and horizontal axes represent for temperature (T) and time (t), respectively. 'X' represents the theoretical optimum, that is, martensite, and 'A' represents the amorphous strain state in the ferroelastic system. See text for discussions of the shapes of the three TTT curves.

ferroic state, for example, the ferroic glass in Figure 1) that is relatively far from the theoretical optimum (X) (for example, long-range ordered domain structures), but the ferroic relaxation (ageing) would be sluggish when compared with the laboratory timescale such that one must reckon with A. There are discussions in the strain glass literature regarding whether the source of the ferroic disorder (also known as nanoscale heterogeneities) at lower temperatures in A is due to a dynamical arrest of the thermally equilibrated ferroic disorder of higher temperatures (strain liquid), or a quenched-in 'diffusive' disorder (chemical) from even higher temperatures[13–15] or both. For this study, however, the exact source of this ferroic disorder is irrelevant. Here it makes no difference whether one is dealing with the ferroic analog of the liquid melt-quench-produced structural glass or the various forms of 'solid-state' amorphization (such as ion implantation, oxidation, stress-induced amorphization and so on) that have not experienced the characteristic liquid-to-glass transition often used in textbooks. The only hypothesis we make in our theory is that the relaxation rate at A is so slow that significant ferroic disorder survives for a period of time that affects the application of interest. An analogy is the native silicon oxide formed by air oxidation on cleaved silicon surfaces, where diffusive relaxation is so slow that the silicon oxide is not transformed to crystalline quartz.

For the convenience of our discussion, we define the relaxation rate R (inverse of relaxation time) as

$$R(T) \equiv \upsilon_{\mathrm{D}} \exp\left(-\frac{Q(T)}{k_{\mathrm{B}}T}\right) \tag{1}$$

where $\upsilon_{\mathrm{D}} \sim 10^{12}\,\mathrm{s}^{-1}$ is a fixed frequency for each attempt, taken as the Debye frequency, and $Q(T)$ is an effective activation energy. To avoid controversy in our terminology, we will use the term 'amorphous ferroics' instead of 'ferroic glasses' to describe the present state A that has more ferroic disorder than X. $Q(T)$ is a lumped parameter[16] containing both the driving force (for example, the drop in the free energy when the native silicon oxide transforms to quartz in the example above) and the microscopic pathway sampling (that is, kinetics). We quantify the driving force by the following:

$$\Delta f(T) \equiv \frac{F(A, T) - F(X, T)}{\text{Total volume}}, \tag{2}$$

where F is the constrained Helmholtz free energy within the metabasin A or X in the $\mathbf{r}^{3N}$ phase space (where N is the number of atoms)

obtained by integrating the partition function within a metabasin:

$$F(A, T) \equiv -k_{\mathrm{B}} T \ln Z(A, T),$$
$$F(A, T) \equiv \int_{\mathbf{r}^{3N} \in \text{basinA}} \mathrm{d}\mathbf{r}^{3N} \exp\left(-\frac{U(\mathbf{r}^{3N})}{k_{\mathrm{B}}T}\right), \tag{3}$$

where $U(\mathbf{r}^{3N})$ is the potential energy. The normalization of Equation (2) by volume is to make the driving force an intensive quantity. Note that Δf has the same unit as stress (MPa), and can be considered a thermodynamic driving force. We can then model the two contributions to $Q(T)$—the driving force dependence and the energy landscape 'ruggedness' dependence—more explicitly by defining a two-variable function as follows:

$$Q(T) \equiv Q(\Delta f(T), T) \tag{4}$$

where the first dependency on the right-hand side is the driving force and the second dependency comes from the microscopic pathway sampling.[17] To accentuate the first dependency, we define an activation volume by the following:

$$\Omega(\Delta f, T) \equiv -\frac{\partial Q}{\partial \Delta f}\Big|_{T \text{ in second entry}}, \tag{5}$$

where 'T in second entry' refers to the T outside Δf that is also a function of temperature. The definitions above are general and apply to both the diffusion-dominated and displacement-dominated atomic relaxations (for an atomistic definition of diffusive/civilian vs displacive/military processes, see refs 18,19). However, the activation volume Ω of displacement-dominated processes (such as deformation twinning) is generally much larger than that of diffusion-dominated processes (such as diffusional creep) because the latter are much more one atom's 'decision' than many atoms' collective action at the saddle point.[20] Ferroic relaxations are classified as displacement-dominated processes and, according to Cross' estimate,[2] involve changes of ferroic order in an $\sim (10\,\mathrm{nm})^3$ volume in relaxor ferroelectrics, which is equivalent to an $\sim 10^4$ atomic volume that is much larger than the Ω of typical atomic diffusion (usually <1 atomic volume[21]). Therefore, the following holds

$$\Omega_{\text{diffusive relaxation}} \ll \Omega_{\text{ferroic relaxation}}. \tag{6}$$

This can have a profound consequence on the TTT behavior. In considering the example of the native oxide again, if a native oxide is amorphous at room temperature, it will not crystallize into quartz as $T \to 0\,\mathrm{K}$. In the liquid melt-quench case, once the opportunity window for crystallization (the TTT nose) is missed, the system ends up as a structural glass at any lower temperatures. We are confident about the eventual amorphous outcome in these two diffusive examples because $\frac{T}{Q(T)}$ and, therefore, the diffusional relaxation rate $R(T)$ in Equation (1) decrease monotonically as $T \to 0\,\mathrm{K}$. This is because as T decreases, although $Q(T)$ may drop, it does not drop as fast as T, and T will reach zero first, giving rise to an infinitely slow relaxation (aging) at $T = 0\,\mathrm{K}$ and a permanent amorphous state. Therefore, once the disorder appears at a specific temperature, the disorder is maintained while the temperature decreases further. As we will show below, this is no longer the case when the activation volume Ω is large enough, that is, the ferroic relaxation can instead accelerate with decreasing temperature, resulting in a decrease in the ferroic disorder in A as the temperature decreases, and eventually the amorphous ferroics may crystallize into X at a lower temperature.

Consider the change in relaxation rate with temperature as follows:

$$\frac{\mathrm{d}}{\mathrm{d}T} \frac{T}{Q(\Delta f(T), T)} = \frac{Q - T\left(\Omega \Delta s_{\mathrm{AX}} + \frac{\partial Q}{\partial T}\big|_{\Delta f}\right)}{Q^2} \tag{7}$$

where

$$\Delta s_{AX} \equiv -\frac{d\Delta f}{dT} \equiv \frac{S(A,T) - S(X,T)}{\text{total volume}} > 0 \qquad (8)$$

is the entropy difference between A and X per volume. The quantity

$$Q - T \left.\frac{\partial Q}{\partial T}\right|_{\Delta f} = \left.\frac{\partial(Q/T)}{\partial(1/T)}\right|_{\Delta f} \equiv H \qquad (9)$$

can be defined as the effective activation enthalpy according to the Gibbs–Helmholtz relation. So we obtain the critical condition for a transition from 'colder is slower' to 'colder is faster':

$$0 \geq \frac{d}{dT}\frac{T}{Q(\Delta f(T),T)} \rightarrow 0 \geq H - T\Omega\Delta s_{AX} \qquad (10)$$

which gives a particularly simple physical picture: if the excess entropy (Δs_{AX}) of A with respect to X within the activation volume Ω exceeds the enthalpic barrier (H) of relaxation between A and the next metabasin A′ (A → A* → A′, where A′ is the next metabasin on the path of aging and A* is the saddle point in between),[20] then the change in the relaxation rate becomes positive upon cooling and the relaxation dynamics will accelerate with decreasing T (that is, colder is faster), and vice versa.

The excess entropy Δs_{AX} can be evaluated from first principles. In the diffusional transformation examples, if A is liquid and X is crystal, from Richard's rule, Δs_{AX} would be ~ k_B per atomic volume. If A is ergodicity-limited to a single vibrational basin, then Δs_{AX} would be the vibrational entropy difference that may reasonably be ~ 0.1 k_B per atomic volume. However, in general, because diffusional transformations have a small activation volume Ω[20], the right hand side of Equation (10) is 'activation enthalpy H-dominated' and cannot turn negative. Thus, the system will stay in the 'colder is slower' regime, and the amorphous state would remain even with a further decreasing T.

However, the case for ferroic materials is quite different and is dependent on defect concentration c. Figure 2 illustrates the effective activation enthalpy H and entropy $T\Omega\Delta s_{AX}$ for ferroics with different values of c at a constant temperature T, which is lower than the thermodynamic equilibrium transition temperature. As c increases, the effective activation enthalpy H for the A → X transition increases (that is, it is more difficult for the A → X transition to take place) because the randomly distributed point defects pose energetic barriers that need to be overcome to form a long-range ordered ferroic state. However, the effective activation entropy $T\Omega\Delta s_{AX}$ has the opposite
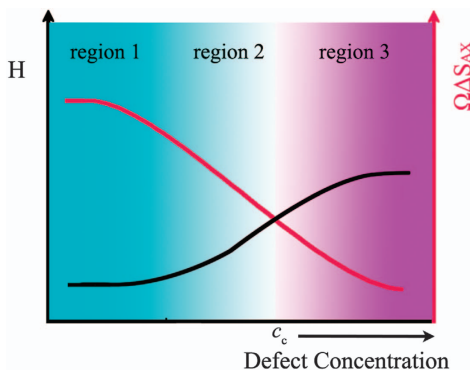
Figure 2 Effective activation enthalpy H (black curve) and effective entropy within activation volume $\Omega\Delta s_{AX}$ (red curve) change along with defect concentration at a certain temperature (schematic). Here c_c represents a critical point defect concentration where 'colder is faster' transfers into 'colder is slower'.

trend. On one hand, there is no huge variation in the magnitude of Δs_{AX} because, as mentioned above, a vibrational entropy difference of ~ 0.1 k_B per atomic volume seems appropriate. On the other hand, the activation volume $\Omega \sim l_c^3$ should decrease with increasing c by a simple geometric scaling argument because more random point defects make the transition less collective. Consequently, we can divide the whole range of the concentration of point defects into two parts. The first part is before the intersection point (c_c in the horizontal axis of Figure 2) of these two curves (region 1 and 2 combined): here the final phase upon cooling to $T = 0$ K is X, and the growth of nanodomains is activation entropy-dominated, thus 'colder is faster'; the second part is after the intersection point (region 3): here the nanodomain growth and coarsening are always activation enthalpy-dominated, thus 'colder is slower', such as in structural glasses (we refer to it as the 'permanent amorphous ferroic' (PAF) state here because the ferroic disorder can survive down to $T \rightarrow 0$ K). The temperature we consider here is lower than the corresponding nucleation temperature, thus, the nanodomains can exist steadily but the whole system is still far from X.

Furthermore, we can divide the former part further into two regions. Below a certain concentration (region 1), a normal first-order ferroic transition takes place. After this concentration (region 2), the parent phase will first jump into a metastable state (A) and then later escape from this state to X through a colder-is-faster nanodomain growth and coarsening. Because this metastable state is in transient disorder (it exists at intermediate temperatures but cannot survive to 0 K), we call it the 'transient amorphous ferroic' (TAF) state. Thus, the standard ultrafast 'almost instantaneous' ferroic transition takes place in region 1, the TAF and spontaneous A → X transition occur in region 2 but before the intersection point and the PAF state appears in region 3.

In summary, because of the two competing activation parameters of comparable magnitude in ferroic transitions, the right-hand side of Equation (10) may turn from 'activation entropy-dominated' to 'activation enthalpy-dominated' as we increase the concentration of point defects, and the ferroic relaxation dynamics would change from 'colder is faster' (leading to TAF) to 'colder is slower' (leading to PAF). Indeed, the plausibility of TAF hinges on the scenario where $Q(T)$ hits zero before T reaches zero, as it is common for displacive processes (dislocation slip, fracture, deformation twinning and so on) to have the so-called 'athermal threshold'[20] Δf_{ath}:

$$Q(\Delta f_{ath}, T > 0) = 0. \qquad (11)$$

If $\Delta f(T_0 > 0) = \Delta f_{ath}$, the ferroic relaxation dynamics would become infinitely fast as $T \rightarrow T_0$ from above. In this case, the amorphous ferroics can never survive below T_0 and therefore, the ferroic disorder must be in the TAF condition (as shown by the horizontal blue line in the TTT diagram in Figure 1). Such accelerating ferroic dynamics with decreasing temperature in amorphous ferroics should also have interesting internal friction signatures[22] above T_0. Please note that ferroic relaxation under a small driving force has been analyzed by Vugmeister *et al*.[23] using a linear-response theory. In the case of a large driving force, however, such dependence becomes the main driver of the novel 'colder is faster' phenomenon discussed above and cannot be ignored.

Numerical simulation
To verify the analytical theory above, we carry out two-dimensional phase field simulations of detailed microstructural changes upon cooling in a generic ferroelastic system that undergoes a cubic to tetragonal martensitic transformation (MT). Three different
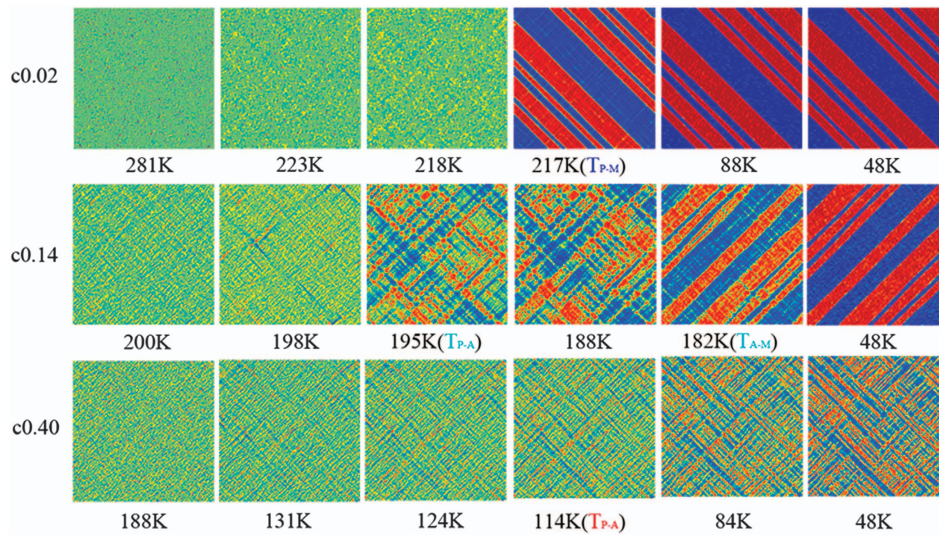
Figure 3 Microstructure evolutions upon cooling in three ferroelastic systems having different defect concentrations, $c=0.02$, 0.14 and 0.40, respectively. Green color in the figures represents the parent phase; blue and red colors represent the two different martensitic variants. The final state of cooling is 48 K.

concentrations of doped point defects are considered and the simulation results obtained are shown in Figure 3. When the point defect concentration $c=0.02$, the first figure in the top row of Figure 3 shows the microstructure of the parent phase (which will be hereafter referred to as austenite) at 281 K, where the green color represents the austenite and the deviations from the green color describe the structural nonuniformities (lattice distortions) associated with martensitic embryos induced by the doped defects. When T decreases to 217 K (T_{P-M}, that is, the austenite to martensite transition temperature), the system shows a sudden appearance of twinned martensitic plates, with equilibrium values (red and blue) of the order parameters introduced in the phase field model to describe the two Bain variants of martensite. This can also be detected by the change in the martensitic volume fraction and its derivative with respect to temperature (Supplementary Figure S1a and b). At T_{P-M}, the martensitic volume fraction shows a sudden jump and then gradually approaches 100%. Correspondingly, a sharp peak appears at T_{P-M} in the derivative of the martensitic volume fraction with respect to T. In addition, the sharp peak shown in the calculated differential scanning calorimetry curve (Supplementary Figure S2) at T_{P-M} clearly indicates an ultrafast 'almost instantaneous' characteristic of the standard MT. After the phase transition, the system has a well-developed long-range-order (LRO) strain pattern consisting of two different martensitic variants in a polytwin structure. The structure is stable till the end of the cooling process at 48 K (see the last figure in the top row of Figure 3). Supplementary Figure S1c and d shows the change in the number of domains upon cooling. At this low doping level ($c=0.02$), the domain number first increases and then decreases to a relatively small value, consistent with the final structural state of the system shown in Figure 3; this state consists of well-developed large martensitic twin domains. Thus, when the concentration is low, point defects cannot prevent the LRO twinning martensite from forming.

When $c=0.40$ (the bottom row of Figure 3), the microstructure changes upon cooling are fundamentally different. There are no sudden changes in the number of domains, domain size and volume fraction of martensite. Although spatial correlations among more mature martensitic domains start to develop upon cooling, leading to tweed-like patterns,[24] the LRO twinning plates never form. The increase in the total martensitic volume fraction starts at a much lower

temperature (~130 K) and is rather slow (Supplementary Figure S1a) upon further cooling compared with the previous case. In addition, it reaches only ~ 35% rather than 100% at the end of cooling. The number of domains starts to increase at the same temperature (~130 K), with the increasing rate (the slope of the domain number vs temperature curve shown in Supplementary Figure S1c) reaching its maximum value at ~ 114 K and the number of domains reaching (gradually, as shown in Supplementary Figure S1b) its maximum value at ~ 68 K (Supplementary Figure S1a). Although the domain number starts to decline upon further cooling, more than 80% of the domains survived at the end of cooling. Thus, when the defect concentration is high, the system ends up in the PAF condition, with a nanoscale ferroic disorder capable of surviving to $T \rightarrow 0\,K$[25–27] that never transforms into the LRO twinning martensite. This is because 'colder is slower' has taken hold and T reaches zero before $Q(T)$ does, as in the relaxation dynamics of conventional structural glass.

The middle row in Figure 3 shows the microstructure evolution in a system in the crossover region on the ferroelastic strain-state phase diagram,[7] that is, the region with a defect concentration of $c=0.14$ in the model system considered in this study. The simulation results show a 'diffuse' MT, that is, the system eventually transforms into the LRO twinning martensite, but the transition occurs in a wide temperature range (~13 K), which is in sharp contrast to that of normal MT that occurs in the system with $c=0.02$. Above 195 K, only martensitic nanodomains exist in the systems, but the peak at temperature T_{P-A} in Supplementary Figures S1b and S2 suggests that individual domains of martensite begin to nucleate and grow rapidly below this temperature; however, no interconnected martensitic plates are formed yet. At 182 K (T_{A-M}), domains are interconnected and LRO twinned martensitic plates emerge. Correspondingly, the second peak appears in Supplementary Figures S1b and S2, suggesting that a transition from a TAF state (a metastable state similar to the last figure in the bottom row of Figure 3) to a normal martensitic structure by 'displacive domain growth and coarsening' has occurred at this temperature. With continued cooling, the internally twinned martensitic structure develops further (with a higher degree of perfection) and remains till the end. In this case, a two-step transition, austenite → TAF state → LRO twinning martensite takes place.
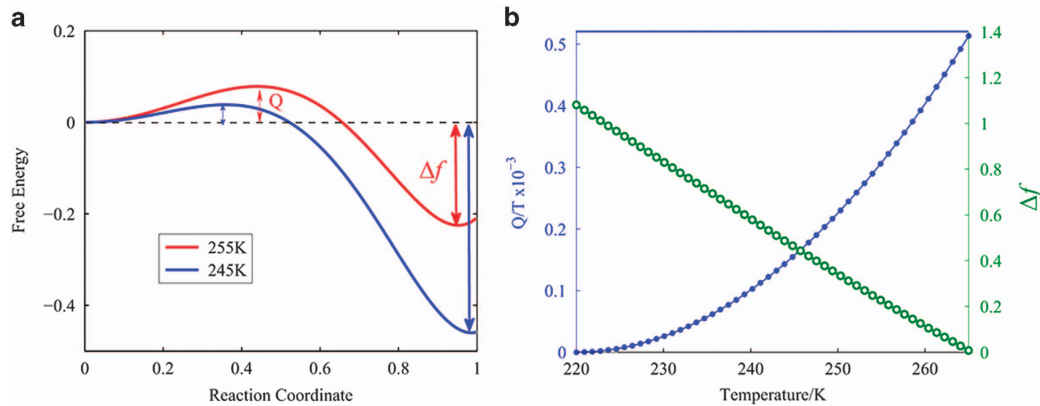
Figure 4 Thermodynamics and kinetics of the ferroelastic system. (**a**) The free energy curves for austenite→martensite transition at 255 and 245 K, respectively. Q is the activation energy and Δf is the driving force. (**b**) The temperature-dependence of Q/T (blue dot line) and Δf (green dot line).

Figure 4a shows the Landau free energy curves of the system at 255 and 245 K. We can see that the activation energy Q decreases, whereas the driving force Δf increases as temperature decreases. Both of these make the MT easier. A detailed analysis of the temperature-dependence of Q/T and Δf is displayed in Figure 4b. Although Δf scales linearly with temperature (the green curve Figure 4b), Q/T is more sensitive to temperature because Q is also a strong function of Δf; thus, $\frac{\mathrm{d}}{\mathrm{d}T}\frac{Q}{T}>0$, which can be readily observed from the blue curve in Figure 4b. Therefore, the MT kinetics will accelerate with decreasing temperature, making the percolation of martensitic domains and formation of LRO twinning plates (that is, spontaneous A to X transition) more observable at lower temperatures.

As was stated earlier, the essential difference between structural glass and amorphous ferroics lies in their TTT curves (Figure 1). There is a single-type C-shaped curve (the red curve) for the structural glass to crystal transition, where the diffusive atomic relaxation process is always 'colder is slower' once the nucleation difficulty is overcome, while three different types of TTT curves can be anticipated for the ferroics at three typical point defect concentration levels, as illustrated schematically in Figure 1. These TTT curves are associated with the additional kinetic difficulty of 'displacive growth and coarsening' that has different characteristics from diffusional processes. The dashed line is a cooling line with a constant cooling rate, and the dark blue, light blue and red curves are for the ferroelastic systems considered in the simulations with a defect concentration of 0.02, 0.14 and 0.40, respectively. When the point defect concentration is low (0.02), a first-order MT takes place at T_0. This transition happens in such a short time that we can almost neglect the role of time, which means that the transition temperature almost remains constant as the cooling rate changes. In this case, the TTT curve is a horizontal line (dark blue). As the point defect concentration increases (at 0.14 for instance), the TTT curve (light blue) has a 'half-C' shape and the behavior of the system becomes quite different. The parent phase (strain liquid) will first transform into an amorphous ferroelastic state (that is, frozen strain disorder) at a temperature slightly lower than T_0. The system remains in such an amorphous state (that is, the TAF state mentioned above) owing to the sluggish 'displacive domain growth and coarsening' within the temperature range (T_0 and T_1), and the amorphous state to martensite transition (the LRO strain state) will take place upon further cooling to temperatures below T_1. The range (T_0 and T_1) where the TAF state exists depends on the specific cooling rate. At a higher defect concentration (for example, $c=0.4$), the TTT curve (red) has a normal C shape. If the cooling rate is large enough (black dashed

line), the observation time t_2 will be smaller than the critical time needed to observe the MT, and thus the cooling line does not intersect with the TTT curve at this doping level. Consequently, we can only observe the austenite→amorphous ferroelastic state transition, and the system will be trapped in a PAF state, with nanoscale ferroic disorder capable of surviving to $T \to 0$ K. Thus, a highly doped ferroelastic system is expected to behave similarly to a structural glass owing to the dominance of the activation enthalpy term in the relaxation kinetics.

CONCLUSION

In conclusion, we have formulated a theoretical framework for analyzing the temperature and defect concentration dependence of ferroic relaxations and ferroic transitions. The framework reveals the nature of the accelerating ferroic dynamics (post-nucleation displacive domain growth and coarsening) upon cooling and unveils a change from 'colder is faster' to 'colder is slower' with an increasing defect concentration. The origin of such a transition arises from the fact that there are two competing activation parameters of potentially comparable magnitude for ferroic dynamics, that is, the activation entropy and activation enthalpy, as a result of the much larger activation volumes of displacive atomic processes compared with those of diffusional processes. When the defect concentration is low, the ferroic relaxation is dominated by the activation entropy, and the relaxation is 'colder is faster'. However, as the defect concentration increases, the activation enthalpy will become dominant and the relaxation kinetics changes to 'colder is slower'. There are two types of ferroic disorders associated with this parametric change: one (TAF) that cannot survive to $T \to 0$ K and transforms to ferroic crystal, and one (PAF) that can survive and transforms to permanent amorphous ferroics or ferroic glasses. These theoretical predictions have been verified by phase field simulations of the microstructural (strain state) evolution during a generic ferroelastic phase transition upon cooling in systems with three different defect concentration levels.

CONFLICT OF INTEREST

The authors declare no conflict of interest.

1 Entel, P., Arroyave, R., Fähler, S., Kainuma, R., Planes, A., Ren, X. & Saxena, A. Ferroic glasses: magnetic, polar and strain glass. *phys. status solidi b* **251**, 1965–1966 (2014).

2 Cross, L. E. Relaxor ferroelectrics. *Ferroelectrics* **76**, 241–267 (1987).

3 Bokov, A. A. & Ye, Z. G. Recent progress in relaxor ferroelectrics with perovskite structure. *J. Mater. Sci.* **41**, 31–52 (2006).

4 Sherrington, D. A spin glass perspective on ferroic glasses. *phys. status solidi b* **251**, 1967–1981 (2014).

5 Sarkar, S., Ren, X. & Otsuka, K. Evidence for strain glass in the ferroelastic-martensitic system Ti 50-x Ni 50+ x. *Phys. Rev. Lett.* **95**, 205702 (2005).

6 Chu, F., Reaney, I. & Setter, N. Spontaneous (zero-field) relaxor–to–ferroelectric-phase transition in disordered Pb (Sc1/2Nb1/2) O3. *J. Appl. Phys.* **77**, 1671–1676 (1995).

7 Zhang, J., Wang, Y., Ding, X., Zhang, Z., Zhou, Y., Ren, X., Wang, D., Ji, Y., Song, M. & Otsuka, K. Spontaneous strain glass to martensite transition in a Ti 50 Ni 44.5 Fe 5.5 strain glass. *Phys. Rev. B* **84**, 214201 (2011).

8 Wang, Y., Huang, C., Wu, H., Gao, J., Yang, S., Wang, D., Ding, X., Song, X. & Ren, X. Spontaneous strain glass to martensite transition in ferromagnetic Ni-Co-Mn-Ga strain glass. *Appl. Phys. Lett.* **102**, 141909 (2013).

9 Ren, X. Strain glass and ferroic glass—unusual properties from glassy nano-domains. *phys. status solidi b* **251**, 1982–1992 (2014).

10 Kartha, S., Castán, T., Krumhansl, J. A. & Sethna, J. P. Spin-glass nature of tweed precursors in martensitic transformations. *Phys. Rev. Lett.* **67**, 3630 (1991).

11 Semenovskaya, S. & Khachaturyan, A. Coherent structural transformations in random crystalline systems. *Acta. Mater.* **45**, 4367–4384 (1997).

12 Zhou, Y., Xue, D., Ding, X., Wang, Y., Zhang, J., Zhang, Z., Wang, D., Otsuka, K., Sun, J. & Ren, X. Strain glass in doped Ti 50 (Ni 50− xDx)(D= Co, Cr, Mn) alloys: implication for the generality of strain glass in defect-containing ferroelastic systems. *Acta. Mater.* **58**, 5433–5442 (2010).

13 Kustov, S., Salas, D., Cesari, E., Santamarta, R., Mari, D. & Humbeeck, J. V. Strain glass revisited. *Mater. Sci. Forum* **738–739**, 274–275 (2013).

14 Kustov, S., Salas, D., Cesari, E., Santamarta, R., Mari, D. & Van Humbeeck, J. Structural anelasticity, elasticity and broken ergodicity in Ni-Ti shape memory alloys. *Acta. Mater.* **73**, 275–286 (2014).

15 Liu, J. & Jin, X. Is 'strain glass' a nanodomain frozen transition? *phys. status solidi b* **251**, 2055–2060 (2014).

16 Kushima, A., Lin, X., Li, J., Eapen, J., Mauro, J. C., Qian, X., Diep, P. & Yip, S. Computing the viscosity of supercooled liquids. *J. Chem. Phys.* **130**, 224504 (2009).

17 Li, J., Kushima, A., Eapen, J., Lin, X., Qian, X., Mauro, J. C., Diep, P. & Yip, S. Computing the viscosity of supercooled liquids: Markov network model. *PLoS ONE* **6**, e17909 (2011).

18 Wang, C.-C., Mao, Y.-W., Shan, Z.-W., Dao, M., Li, J., Sun, J., Ma, E. & Suresh, S. Real-time, high-resolution study of nanocrystallization and fatigue cracking in a cyclically strained metallic glass. *Proc. Natl Acad. Sci. USA* **110**, 19725–19730 (2013).

19 Mao, Y., Li, J., Lo, Y.-C., Qian, X. & Ma, E. Stress-driven crystallization via shear-diffusion transformations in a metallic glass at very low temperatures. *Phys. Rev. B* **91**, 214103 (2015).

20 Li, J. The mechanics and physics of defect nucleation. *MRS Bull.* **32**, 151–159 (2007).

21 Zhu, T. & Li, J. Ultra-strength materials. *Prog. Mater. Sci.* **55**, 710–757 (2010).

22 Hamzić, A. & Campbell, I. [The spin glass to ferromagnetic order transition in AuFe alloys]. *J. Phys. Lett.* **42**, 309–312 (1981).

23 Vugmeister, B. & Rabitz, H. Dynamics of interacting clusters and dielectric response in relaxor ferroelectrics. *Phys. Rev. B* **57**, 7581 (1998).

24 Kartha, S., Krumhansl, J. A., Sethna, J. P. & Wickham, L. K. Disorder-driven pretransitional tweed pattern in martensitic transformations. *Phys. Rev. B* **52**, 803 (1995).

25 Zhang, Z., Wang, Y., Wang, D., Zhou, Y., Otsuka, K. & Ren, X. Phase diagram of Ti 50−x Ni 50+x: Crossover from martensite to strain glass. *Phys. Rev. B* **81**, 224102 (2010).

26 Semenovskaya, S. & Khachaturyan, A. G. Coherent structural transformations in random crystalline systems. *Acta Mater.* **45**, 18 (1997).

27 Kartha, S., Castan, T., Krumhansl, J. A. & Sethna, J. P. Spin-glass nature of tweed precursors in martensitic transformations. *Phys. Rev. Lett.* **67**, 4 (1991).

Supplementary information of

Accelerating Ferroic Ageing Dynamics upon Cooling

Junyan Zhang[1,2,6], Yunwei Mao[1,2,7], Dong Wang[1,2], Ju Li[1,2,3,4]* Yunzhi Wang[1,2,5]*

[1] Frontier Institute of Science and Technology, Xi'an Jiaotong University, Xi'an 710049, China
[2] State Key Laboratory for Mechanical Behavior of Materials, Xi'an Jiaotong University, Xi'an 710049, China

[3] Department of Nuclear Science and Engineering, Massachusetts Institute of Technology, Cambridge, MA 02139, USA

[4] Department of Materials Science and Engineering, Massachusetts Institute of Technology, Cambridge, MA 02139, USA

[5] Department of Materials Science and Engineering, The Ohio State University, 2041 College Road, Columbus, OH 43210, USA

Present address: [6] Department of Chemical Engineering, Northeastern University, Boston, MA 02115, USA
[7] Department of Mechanical Engineering, Massachusetts Institute of Technology, Cambridge, MA 02139, USA

*Corresponding authors: liju@mit.edu; wang.363@osu.edu

S1. Phase field simulation details

A generic cubic→tetragonal martensitic transformation in 2D is considered. The two crystallographically equivalent and hence energetically degenerate Bain paths generate two deformation variants, which can be described by two non-conserved order parameter fields, $\eta_1(r)$, and $\eta_2(r)$, respectively, in the Landau free energy, where r is the coordinate vector. Any given microstructural state in the system can be described by local values of these two order parameter fields, e.g., $(\eta_1, \eta_2) = (0,0)$ represents the austenite and $(\eta_1, \eta_2) = (1,0)$, or $(0,1)$ represents one of the two deformation variants of the martensitic phase, respectively.

$$\varepsilon_{ij}^0(\vec{r}) = \varepsilon_{ij}^{01}\eta(\vec{r})_1^2 + \varepsilon_{ij}^{02}\eta(\vec{r})_2^2$$

where the stress free transformation strains of the two deformation variants are $\varepsilon_{ij}^{01} = \varepsilon_0 \begin{pmatrix} 1 & 0 \\ 1 & \bar{1} \end{pmatrix}$ and $\varepsilon_{ij}^{02} = \varepsilon_0 \begin{pmatrix} \bar{1} & 0 \\ 1 & 1 \end{pmatrix}$. The total energy of the system consists of two parts: the chemical free energy F_{chem} and the elastic strain energy E_{el}. The former one can be expressed in the form of: $F_{chem} = \int d^2r \left[\frac{1}{2}\beta(\nabla\eta_1)^2 + \frac{1}{2}\beta(\nabla\eta_2)^2 + f(\eta_1,\eta_2) \right]$, where the first two terms in the square blanket are the non-local gradient energy terms with β being the gradient energy coefficient and the last term is the "local" chemical free energy described with 6-order Landau Polynomial(1):

$$f(\eta_1,\eta_2) = \frac{1}{2}A_{10}(\eta_1{}^2 + \eta_2{}^2) - \frac{1}{4}A_2(\eta_1{}^4 + \eta_2{}^4) + \frac{1}{4}A_3(\eta_1{}^2 + \eta_2{}^2)^2$$
$$+ \frac{1}{6}A_4(\eta_1{}^2 + \eta_2{}^2)^3$$

($A_{10} = A_1^{00}(T - T_0)$, A_2 to A_4 are the expansion coefficients. In our simulation, $A_1^{00} = 0.05$, $T_0 = 220$, A_2=30, A_3=19, A_4=10). The second part of the total energy, the elastic strain energy, is given by Khachaturyan (1, 2):

$$E_{el} = \frac{1}{2}C_{ijkl}\sum_{p=1}^{2}\sum_{q=1}^{2}\varepsilon_{ij}^{00}(p)\varepsilon_{ij}^{00}(q)\int d^3r \eta_p^2(r,t)\eta_q^2(r,t)$$
$$- \frac{1}{2}\sum_{p=1}^{2}\sum_{q=1}^{2}\int \frac{d^2k}{(2\pi)^2}B_{pq}\left(\frac{\mathbf{k}}{k}\right) \times \{\eta_p^2(r,t)\}_{\mathbf{k}}\{\eta_q^2(r,t)\}_{\mathbf{k}}^*$$

If the system is doped with point defects, whose role can be generalized as the global transition temperature effect (GTTE) and local field effect (LFE)(3), the total free energy only needs to be revised in the "local" chemical free energy term as:

$$f(\eta_1,\eta_2) = \frac{1}{2}A_1(\eta_1{}^2 + \eta_2{}^2) - \frac{1}{4}A_2(\eta_1{}^4 + \eta_2{}^4) + \frac{1}{4}A_3(\eta_1{}^2 + \eta_2{}^2)^2 + \frac{1}{6}A_4(\eta_1{}^2 + \eta_2{}^2)^3$$
$$- \eta_{loc}(1)\left[A_{10}\eta_1 - \frac{1}{3}(A_2 - A_3)\eta_1{}^3 + A_3\eta_2{}^2\eta_1 + \frac{1}{5}A_4\eta_1{}^5 + A_4\eta_2{}^4\eta_1 + \frac{2}{3}A_4\eta_2{}^2\eta_1{}^3 \right]$$
$$- \eta_{loc}(2)\left[A_{10}\eta_2 - \frac{1}{3}(A_2 - A_3)\eta_2{}^3 + A_3\eta_1{}^2\eta_2 + \frac{1}{5}A_4\eta_2{}^5 + A_4\eta_1{}^4\eta_2 + \frac{2}{3}A_4\eta_1{}^2\eta_2{}^3 \right]$$

where $A_1 = A_{10} + b \cdot \bar{c}$ (b is defect strength and $\bar{c}$ is average defect concentration of the whole system) in the firstterm describes the LTTE, and $\eta_{loc}(1)$ and $\eta_{loc}(2)$ in the last two terms describe the LFE, which are local random fields created by the point defects. One possible physical origin of the LFE is lattice distortion caused by doped point defects, resulting in symmetry breaking of the Landau free energy(4). The stochastic time-dependent kinetic equation is used to describe the temporal evolution of the system microstructure: $\eta_p(r, t + \Delta t) = \eta_p(r,t) + (d\eta_p(r,t)/dt)\Delta t$, where $\frac{d\eta_p(r,t)}{dt} = -M\left(\delta F/\delta\eta_p(r,t)\right) + \xi_p(r,t), p = 1,2$. $\xi_p(r,t)$ is thermal fluctuations, which is produced by a random number generator. The kinetic equation is solved numerically in a

computational cell consisting of 256 × 256 grid sites with periodical boundary conditions applied in both dimensions and macroscopic strain at the boundary is kept zero.

The length scale in our simulation can be estimated by the formula: $\frac{\Delta F}{\Delta F^*} = (\gamma \times dx)/(\gamma^* \times dx^*)$, where ΔF is the free energy between austenite and martensite in experiments, γ is the interfacial energy for coherent face in experiments, and dx is the character length scale in experiment. The physical quantities with star *, ΔF^*, γ^* and dx^*, are the corresponding quantities in simulation. Then $l_0=dx/dx^*$ is the length unit in simulation. Here we assume the interfacial energy for coherent face to be 0.05J/m² and the chemical free energy ΔF for martensitic system is about -1.85×10^6J/m³. Therefore, l_0~0.9nm, meaning one grid length in simulation equals to about 0.9nm in experiment.

S2. Structural analysis of the ferroelastic systems in cooling process

Figure S1 analyzes the structural changes upon cooling for systems with different defect concentrations from 0.02 to 0.40 (dimensionless), equivalent to 0.00222 to 0.04444 (at.%) in dimensional concentration unit. The dimensionless defect concentration, c, can be converted to mole fraction, x, by $x=c*a_0^2/(l_0^2)$ (1), l_0 (0.9nm) is the length scale and a0 is the lattice parameter (~ 0.3nm for NiTi system). A step cooling process was used in our simulations. We run the system under each temperature for enough time steps in order to reach the equilibrium state (volume fraction change is less than 0.05%, approximately for 20,000 steps in our simulations); then decrease the temperature with ΔT (1K) and repeat the procedure until the lowest temperature considered. The results are shown in Fig. S1.
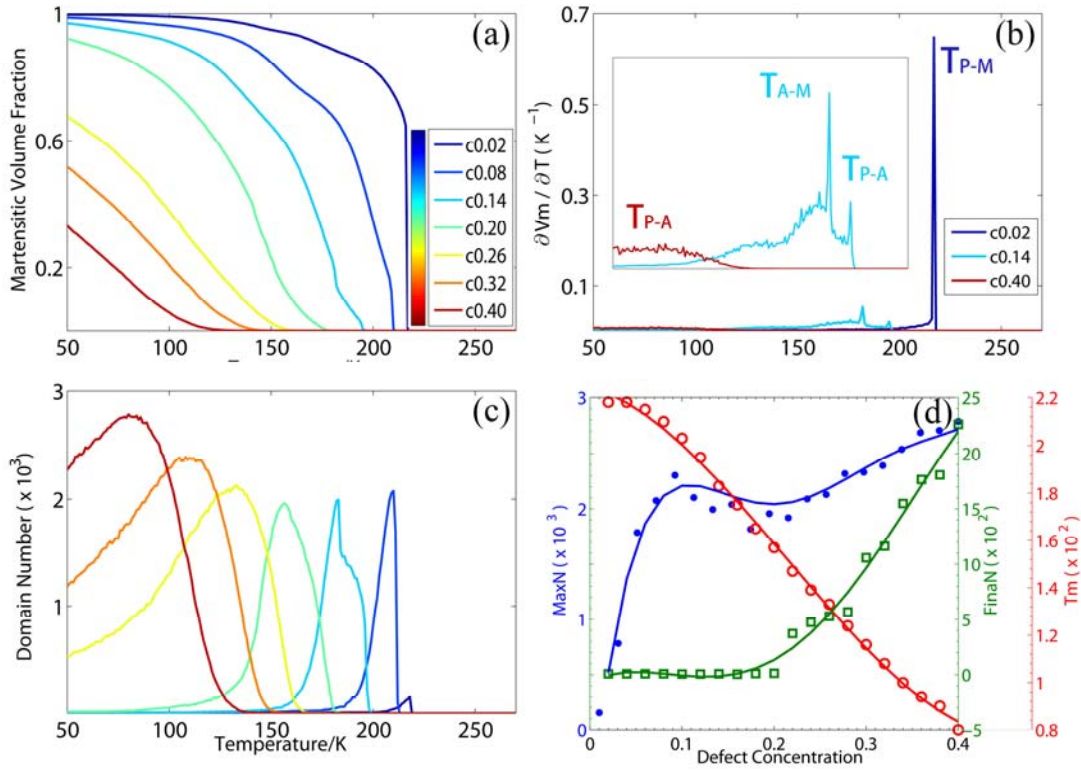
Fig. S1 Structural analysis of ferroelastic systems under different defect concentrations from 0.02 to 0.40. (a) depicts martensitic volume fraction change along with temperature. The defect concentration of each line is indicated by the color bar. (b) is the derivative of martensitic volume fraction with respect to temperature when c=0.02, 0.14 and 0.40. Part of (b) is enlarged in the inserted figure. (c) is the domain number change along with temperature. (d) shows the maximum domain number (MaxN, the blue curve), final domain number (FinaN, the green curve), and the critical temperature corresponding to MaxN (Tm, the red curve) with respect to defect concentration. (a)-(c) share the same color bar.

S3. DSC results of the systems

Furthermore, we calculated the DSC curves of three typical systems (c=0.02, 0.14 and 0.40) in the cooling process. The results are shown in Fig. S2. We can see that for typical martensitic transition, there is a sharp peak indicating the first order martensitic transition. For intermediate concentraion, there are two peaks, one for austenite to amorphous transition at T_{P-A} and the other for amorphous to martensitic transition at T_{A-M}, whereas for a typical amorphization process, there is only one diffuse peak at the transitional temperature.
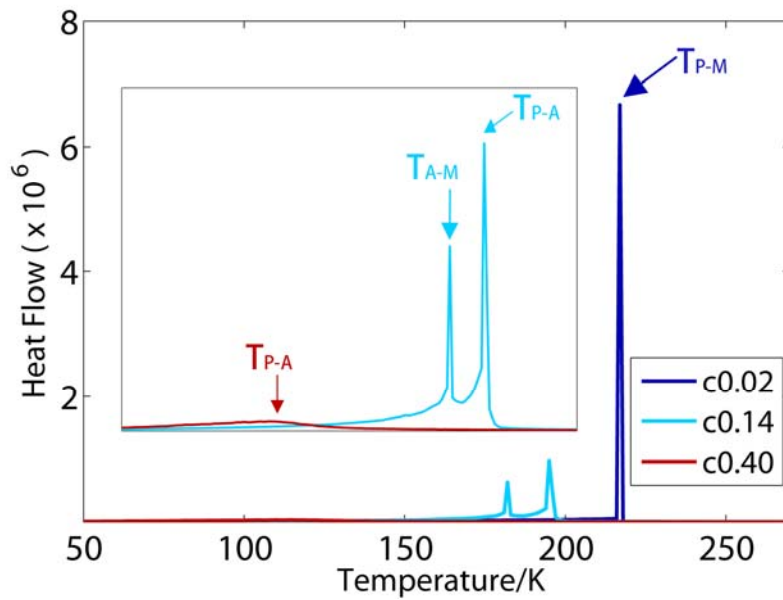
Fig. S2 DSC curves of ferroelastic systems with three typical defect concentrations 0.02, 0.14 and 0.40

1. Semenovskaya S & A.G. K (1997) Coherent structural transformations in random crystalline systems. *Acta Materialia* 45(10):18.
2. Khachaturyan AG (1983) Theory of structural transformations in solids.
3. Levanyuk AP & Sigov AS (1988) Defects and structural phase transitions.
4. Wang D, Wang Y, Zhang Z, & Ren X (2010) Modeling Abnormal Strain States in Ferroelastic Systems: The Role of Point Defects. *Physical Review Letters* 105:4.